Proceedings of the ASME 2012 International Design Engineering Technical Conferences & Computers and Information in Engineering Conference
IDETC/CIE 2012
August 12-15, 2012, Chicago, IL, USA

DETC2012-70233

CORRELATION OF ATOMIC FORCE MICROSCOPY TAPPING FORCES TO MECHANICAL PROPERTIES OF LIPID MEMBRANES

Nicole Shamitko-Klingensmith
Graduate Student
West Virginia University
Department of Chemistry
Morgantown, WV, USA

Kelley M. Wambaugh
Undergraduate Student
West Virginia University
Department of Chemistry
Morgantown, WV, USA

Kathleen A. Burke
Graduate Student
West Virginia University
Department of Chemistry
Morgantown, WV, USA

George J. Magnone
Undergraduate Student
West Virginia University
Department of Chemistry
Morgantown, WV, USA

Justin Legleiter
Assistant Professor
West Virginia University
Department of Chemistry
Morgantown, WV, USA
justin.legleiter@mail.wvu.edu

ABSTRACT

There is considerable interest in measuring, with nanoscale spatial resolution, the physical properties of lipid membranes because of their role in the physiology of living systems. Due to its ability to nondestructively image surfaces in solution, tapping mode atomic force microscopy (TMAFM) has proven to be a useful technique for imaging lipid membranes. However, further information concerning the mechanical properties of surfaces is contained within the time-resolved tip/sample force interactions. The tapping forces can be recovered by taking the second derivative of the cantilever deflection signal and scaling by the effective mass of the cantilever; this technique is referred to as scanning probe acceleration microscopy. Herein, we describe how the maximum and minimum tapping forces change with surface mechanical properties. Furthermore, we demonstrate how these changes can be used to measure mechanical changes in lipid membranes containing cholesterol.

1. INTRODUCTION

Of particular need are technologies to quantitatively and temporally monitor, track, and/or characterize mechanical properties of cellular and subcellular surfaces with nanoscale spatial resolution in an aqueous environment. One strategy to accomplish this goal is to reconstruct the time-resolved force interaction between the tip and surface during tapping mode operation. The time-resolved tip/sample force during tapping contains information analogous to that obtained from the standard force curve experiment. As a result, recent AFM technique development efforts have been focused on reconstructing tip/sample forces while imaging in the tapping mode [1-6].

While tapping mode AFM has long been established as a non-invasive, high resolution imaging technique, the tip/sample interaction can also provide information on adhesion, stiffness, energy dissipation, and chemical composition (with the use of chemically functionalized tips). As we have shown, the instantaneous tip/sample force can be recovered by taking the second derivative of the cantilever deflection signal after applying appropriate filters. This technique is referred to as scanning probe acceleration microscopy (SPAM), and it is capable of operating in aqueous solution [2]. Here, we present a series of simulations to determine how mechanical properties of surfaces change features of the tip/sample force interactions during a tapping mode AFM experiment in solution. We apply these insights to the study of lipid bilayer patches consisting of total brain lipid extract (TBLE) and various amounts of exogenous cholesterol.

2. METHODS

2.1 Simulation

Numerical simulations of fluid TMAFM experiments were performed using MATLAB and SIMULINK (Math Works Inc. Natick, MA.). In these simulations, the cantilever was modeled as a single degree of freedom damped driven harmonic oscillator [7, 8].

$$m_{eff}\ddot{z} + b\dot{z} + k[z - D_0 + a_0 \sin(\omega t)] = F_{ext} \quad (1)$$

where m_{eff} is the effective mass of a cantilever, b is the damping coefficient, k is the cantilever spring constant, a_0 is the drive amplitude, ω is the drive frequency, D_0 is the resting position of the cantilever base, F_{ext} is the tip/sample force, and z is the position of the cantilever with respect to the surface. During tapping mode operation, the cantilever oscillation results in a continually changing separation distance between the probe tip and sample surface, with the probe tip briefly contacting the surface during each oscillation cycle. This results in two tip/sample interaction regimes: 1) at large separation distance when the tip and surface are not in contact and 2) when the tip and surface are in contact during the tapping event. For large tip/sample separation distance, the external force can be approximated using the van der Waals interaction between a sphere and flat surface [9]:

$$F_{ext} = \frac{HR_{tip}}{6z^2} \quad \text{for } z > a_{DMT}\,, \qquad (2)$$

where H is the Hamaker constant, R_{tip} is the tip radius, and a_{DMT} is the interatomic distance parameter of a Derjaguin-Muller-Toporov (DMT) potential [10]. At the bottom of each oscillation cycle, the probe tip contacts the surface when the separation distance z is smaller than the interatomic distance (a_{DMT}). Under these conditions, the tip/sample force can be described by a DMT potential,

$$F_{ext} = \frac{4}{3\pi\kappa_{eff}}\sqrt{R}(a_{DMT} - z)^{3/2} - \frac{HR_{tip}}{6{a_{DMT}}^2} \quad for\ z \le a_{DMT} \quad (3)$$

with

$$\kappa_{eff} = \frac{1-{\upsilon_{tip}}^2}{\pi E_{tip}} + \frac{1-{\upsilon_{sample}}^2}{\pi E_{sample}} \qquad (4)$$

where E_{tip}, ν_{tip} and E_{sample}, ν_{sample} are, respectively, the Young's modulus and Poisson coefficient of the tip and the sample.

While it has been shown that the second mode of the cantilever can play a significant role in cantilever motion near surfaces in fluids [11], we make the assumption that such contributions from the second mode are negligible [12]. By incorporating the contributions from the second mode of the cantilevers motion into the model, the resulting error in the forces will be decreased by 10-15% [11]. However for the purposes of this study, they are neglected because the goal is to observe general relationships between the physical properties of a surface and tip/sample forces. In practice, AFM monitors the deflection of the cantilever rather than its position. While the difference between the position and deflection signal is minimal for systems characterized by high values of Q (such as tapping mode operation in air), these signals differ drastically in low Q systems such as observed in fluid tapping AFM [11, 13, 14]. Therefore, we monitored the deflection (y) as given by:

$$y = z - D_0 + a_0 \sin(\omega t). \qquad (5)$$

The model also contains a feedback loop equipped with an integral gain which allows for a more complete simulation of the scanning process in tapping mode AFM. The feedback loop was implemented by measuring the cantilever amplitude, comparing it to the specified set point, and adjusting the cantilever position with respect to the surface to maintain the set point using an integral gain. The cantilever amplitude was measured by inspecting the cantilever position signal over the length of one oscillation cycle using signal processing tools available in SIMULINK. This feature allows for simulating the process of acquiring an AFM scan line in which a well-defined feature is contained by feeding predetermined surface topography information into the model. The effect of altered sample Young's modulus on the imaging process can also be explored by changing the inputs into Equation 4 and feeding the result into Equation 3. Changes in the adhesive properties of a surface can be modeled by adjusting the Hamaker constant in Equations 2 and 3 because the Hamaker constant is related to the surface free energy (γ) between two materials by:

$$\gamma = \frac{H}{24\pi a_{DMT}} \approx \frac{H}{2.1\times10^{-21}}\,. \qquad (6)$$

This equation can be used to determine the surface free energy between the cantilever tip and the sample surface, where the Hamaker constant describes two surfaces interacting in a medium [15]. These changes in Young's modulus and the Hamaker constant can be synchronized with the predetermined surface topography to model the imaging process on a wide array of scenarios. Here, a topography consisting of a 5 nm plateau with varying physical properties was used as a model surface so that the effects of Young's modulus and the Hamaker constant on tip/sample force could be simulated.

2.2 Experimental

Lyophilized TBLE (Avanti Polar Lipids) and cholesterol (Avanti Polar Lipids) were dissolved in chloroform (ACROS Organics). These chloroform solutions were used to make appropriate mixtures of TBLE and cholesterol. The chloroform was removed under vacuum, and the resulting films were re-suspended in phosphate buffered saline (PBS) at pH 7.3 and a concentration of 1 mg/ml. To promote vesicle formation, the resulting solutions underwent five sequential freeze-thaw cycles using liquid nitrogen followed by sonication for 30 minutes at 40°C. The resulting stock solution was diluted 50x

and 35 µl was injected directly into the AFM fluid cell onto a freshly cleaved mica surface. Small bilayer patches appeared on the mica surface after a short period of time, typically within an hour.

In situ AFM experiments were preformed with a Nanoscope V Multimode scanning probe microscope (Bruker, Santa Barbara, CA) with a tapping fluid cell and a V shaped silicon nitride cantilever with a spring constant of 0.27 N/m. Images were acquired at scan rates of 1.95 Hz and cantilever drive frequencies ranging from approximately 8-9 kHz. Images were captured at 5 x 1.25 µm and 512 x 128 pixel resolution and a set-point ratio of 0.8.

SPAM analysis was used to reconstruct every tapping event during AFM imaging as described [2]. Briefly, cantilever deflection trajectories were simultaneously captured during imaging through an AFM signal access module (Bruker) by using a CompuScope 14-Bit A/D Octopus data acquisition card (Gage Applied Technologies, Lachine, QB, Canada) and custom-written software. Trajectories were captured at 2–5 MS/s and 14-bit resolution with a resolution of 1–2 V. The trajectory of the cantilever was filtered using a Fourier transform based harmonic comb filter. Once a filtered deflection signal is obtained, the second derivative of the filtered cantilever deflection trajectory is taken and divided by the effective mass, m_{eff}, of the cantilever to obtain the time-resolved based tapping force between the tip and sample. Thermal tuning was used to determine the m_{eff} of the cantilever by measuring the cantilevers displacement in response to thermal fluctuations. By examining the data in the frequency domain near the cantilevers resonance frequency, the spring constant was estimated from the power spectral density of the thermal fluctuations [16].

3. RESULTS AND DISCUSSION

In an effort to understand the effect of mechanical surface properties on the time-resolved tip/sample tapping force, single degree of freedom simulations were performed with typical experimental parameters and properties of commercially available silicon nitride cantilevers. These parameters and cantilever properties were: drive frequency of 8-10 kHz, spring constant of 0.5 N/m, free amplitude of 25 nm, and a set point ratio of 0.7 (tapping amplitude of 14 nm). These simulations employed a feedback loop to actively maintain the set point ratio while scanning the cantilever across a model surface, and simulation scan parameters were further chosen to correspond to imaging a 2 µm line with a scan rate of 2 Hz. The model surface employed in these simulations contained a 5 nm step (approximate height of a lipid bilayer) with a Young's moduli of 30 GPa and a Hamaker constant of 3.5 aJ surrounding the step. For each individual simulation, the Young's modulus and Hamaker constant were varied on the step.

To verify the validity of the model, force and deflection trajectories of a single oscillation cycle were compared to those

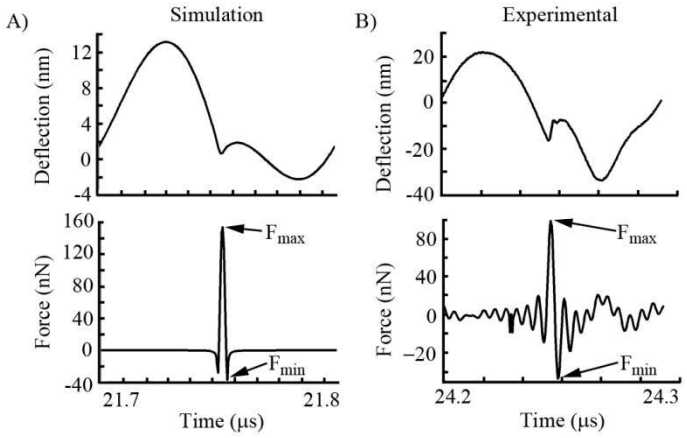

Figure 1. Comparison of the cantilever deflection trajectory and tip/sample force interaction for one oscillation cycle from (A) numerical simulations and (B) experiment. F_{max} and F_{min} are indicated for both the simulation and experiment.

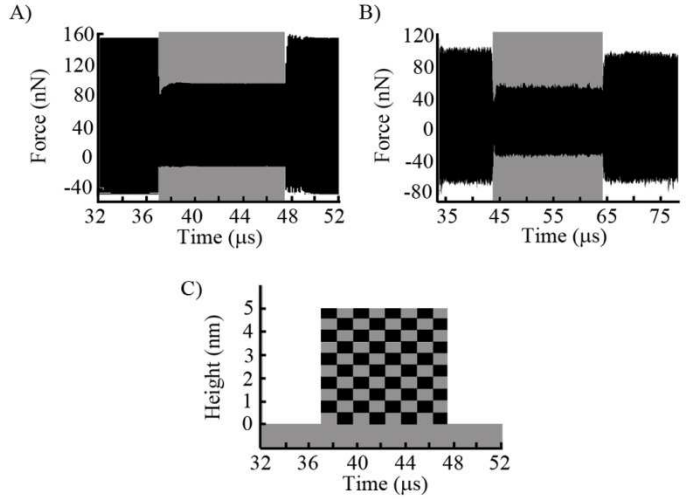

Figure 2. Comparison of tip/sample force interactions over an entire scan line between (A) numerical simulations and (B) experiment. The simulation used a surface topography indicated in (C), in which the area (checkered) of the 5 nm step had E = 20 GPA and H = 0.35 aJ. Before and after the step, E = 30 GPa and H =3.5 aJ. The experimental force trajectory was recovered from a scan line in which a lipid bilayer patch on mica (which is exposed at the beginning and end of the scan line) was imaged. The area of the force trajectory representing imaging the soft step in simulation or lipid bilayer in experiment are represented by gray shading in (A) and (B) respectively.

obtained in experiment (Figure 1). The model captures the characteristic anharmonic deflection trajectory of tapping mode AFM in solution for one oscillation cycle. The tip/sample force

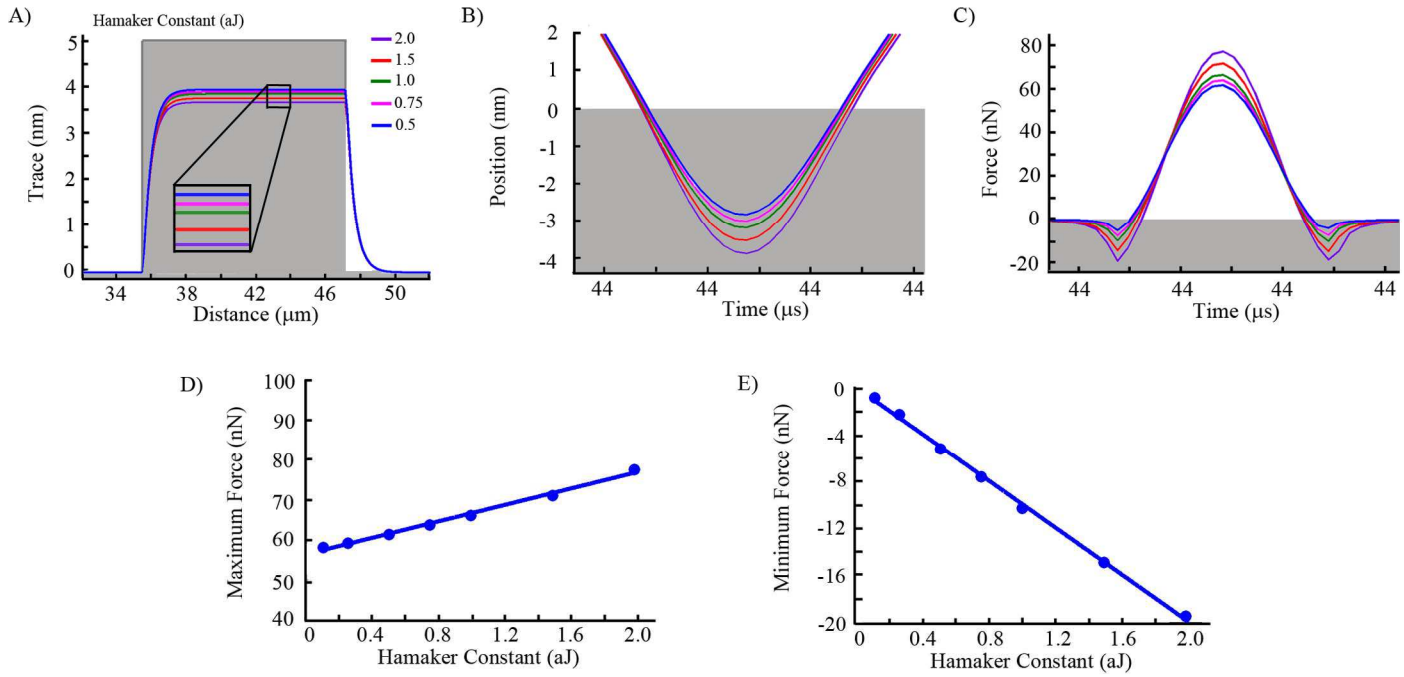

Figure 3. Simulations demonstrating the role of the Hamaker constant on the measured topography and tip/sample interaction forces. (A) The measured topography of a soft step on a hard substrate with varying Hamaker constant, (B) the position of the cantilever with respect to the sample surface zoomed in around the tapping event, and (C) the tip/sample force zoomed in around the tapping event are shown. The (D) F_{max} and (E) F_{min} of the tapping event plotted as a function of the Hamaker constant.

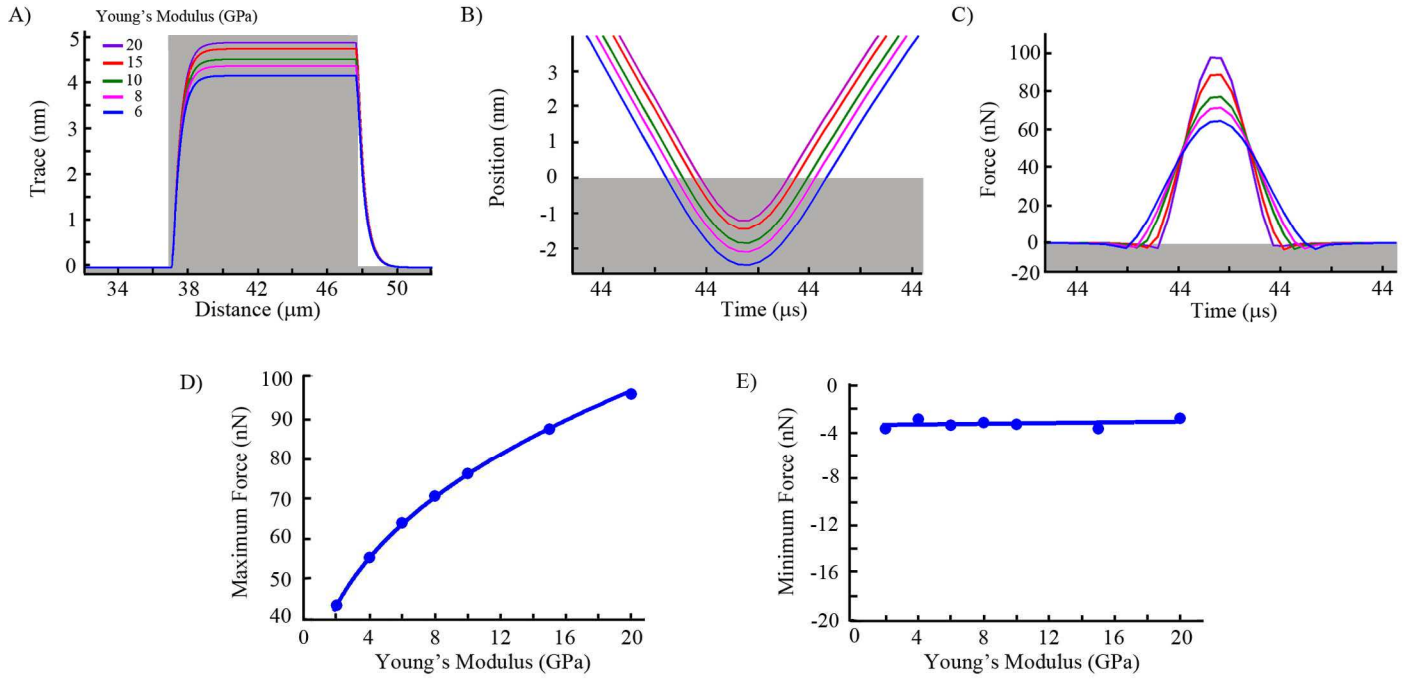

Figure 4. Simulations demonstrating the role of the Young's modulus on the measured topography and tip/sample interaction forces. (A) The measured topography of a soft step on a hard substrate with varying Young's modulus, (B) the position of the cantilever with respect to the sample surface zoomed in around the tapping event, and (C) the tip/sample force zoomed in around the tapping event are shown. The (D) F_{max} and (E) F_{min} of the tapping event plotted as a function of the Young's modulus.

interaction obtained by the simulation also corresponds well with the experimentally obtained tip/sample force during one oscillation cycle as recovered by the SPAM technique. Based on these simulations, the maximum tapping force (F_{max}) is defined as the peak or largest positive force experienced between the tip and surface, and the minimum tapping force (F_{min}) per oscillation cycle is defined as the peak or largest negative force experienced between the tip and surface. Both F_{max} and F_{min} are indicated in Figure 1. Furthermore, if the Young's modulus and Hamaker constant are reduced on the step portion of the model surface, the simulated tip/sample force trajectory associated with the entire scan line can capture features of the tip/sample forces associated with imaging a supported lipid bilayer on mica (Figure 2). These features include a smaller F_{max} and F_{min} associated with imaging the model step in simulation or the lipid bilayer in experiment.

To determine the effect of altering the surface free energy between the tip and surface, simulations were run with variations in the value of the Hamaker constant (based on Equation 6) on the step region of the model surface while keeping all other parameters constant (Figure 3). The Young's modulus was 30 GPa before and after step, and 6 GPa on the step. While the true height of the model step was 5 nm, the measured height of the step during simulation was consistently smaller due to compliance. As the Hamaker constant was increased from 0.5 to 2 aJ, the step became more compressed (smaller measured height Figure 3A). The increased Hamaker constant resulted in a larger attractive force between the tip and surface, which resulted in the tip pushing further into the surface, as can be seen from plotting the position of the tip with respect to the surface (Figure 3B). However, the contact time did not appreciably change. This larger Hamaker constant resulted in larger attractive forces during the start and end of a tapping event (Figure 3C); however, the total force per oscillation cycle must be maintained by the feedback loop to achieve surface imaging. As a result, the F_{max} also increases with increasing Hamaker constant (Figure 3C). The large F_{max} is a result of increased repulsive force due to the larger compression of the surface with larger values of Hamaker constant, which increases the force associated with the Hertzian term in Equation 3. The increase in F_{max} compensates for the increased negative forces to maintain a constant total force per oscillation cycle. As a result, both the F_{max} and F_{min} increase in magnitude linearly with increases in the Hamaker constant; however, the sign of the forces is different (Figure 3 D and E).

To determine the effect of altering the Young's modulus of the surface on the tip/sample force interaction, simulations were run with several different values of the Young's modulus on the step region of the model surface while keeping all other parameters constant (Figure 4). As was the case previously, the simulated measured height of the step was smaller than the true 5 nm height. The measured height of the step during simulation decreased with smaller values of the Young's modulus due to the increased compliance of the surface (Figure 4A), and the tip pushed further into the surface on the softer samples (Figure 4B). However, the contact time between the tip and surface during each tapping event increased with smaller values of Young's modulus. An increased Young's modulus did not result in a larger attractive force between the tip and surface, but the F_{max} increased despite not pushing as far into the surface (Figure 4C). Rather, the increased F_{max} resulted from the κ_{eff} term in Equation 3. This larger F_{max} was compensated for by the shorter contact time, so that the total force per oscillation cycle remained constant for different values of Young's modulus. As a result, only the magnitude of the F_{max} increases with larger values of Young's modulus, and this increase can be described by a power law (Figure 3D). The F_{min} is unresponsive to changes in the Young's modulus (Figure 3E).

Collectively, the simulations with varying values of the Hamaker constant or Young's modulus demonstrate that unique features of the tip/sample tapping force can be used to glean information about specific surface properties. For example, the F_{min} changes linearly with increases in the Hamaker constant, and thus the adhesive force between the tip and surface. The changes in F_{min} are independent of the Young's modulus. While F_{max} is dependent on both the Hamaker constant (linearly) and Young's modulus (power law), it can still be used to determine changes in the Young's modulus. This is because the contribution to F_{max} from the Hamaker constant can be estimated from F_{min}. While a set point of 0.7 was chosen for these simulations, these conclusions are valid for differing set point ratios where set points ranging from 0.8-0.6 are optimal for our imaging purposes. At a set point of 0.9, the same relationships between surface properties and tip/sample forces may not be observed due to the fact that the tip is barely making contact with the surface [1].

We next use SPAM to reconstruct the force associated with every tapping event while imaging supported TBLE bilayers with various amounts of cholesterol (100% TBLE; 90% TBLE + 10% cholesterol; 80% TBLE + 20% cholesterol). Using the simulation results, we were able to determine the mechanical impact of cholesterol on the lipid bilayer patches. To simplify analysis between samples, the same cantilever was used for all experiments presented. Also, several key imaging parameters were maintained between experiments, i.e., a constant drive amplitude, free amplitude, and set point ratio. Based on previous reports, this should maintain a constant total tip/sample force per oscillation cycle as based on the following equation [17]:

$$F_{total} \approx 0.5\, k\, a_0 \left(\frac{\Delta A}{A_0}\right) \qquad (7)$$

Furthermore, only patches of lipid bilayer supported on a mica surface were used for this study. The forces associated with imaging the exposed mica can be used as an internal reference based to normalize for small variations in the tip/sample force interaction [1].

Height images, profiles, and histograms reveal that as the exogenous cholesterol is increased from 0% to 20% that the measured height of the bilayer systematically decreased from 3.7 nm to 2.8 nm (Figure 5 A-C). Based on our simulations,

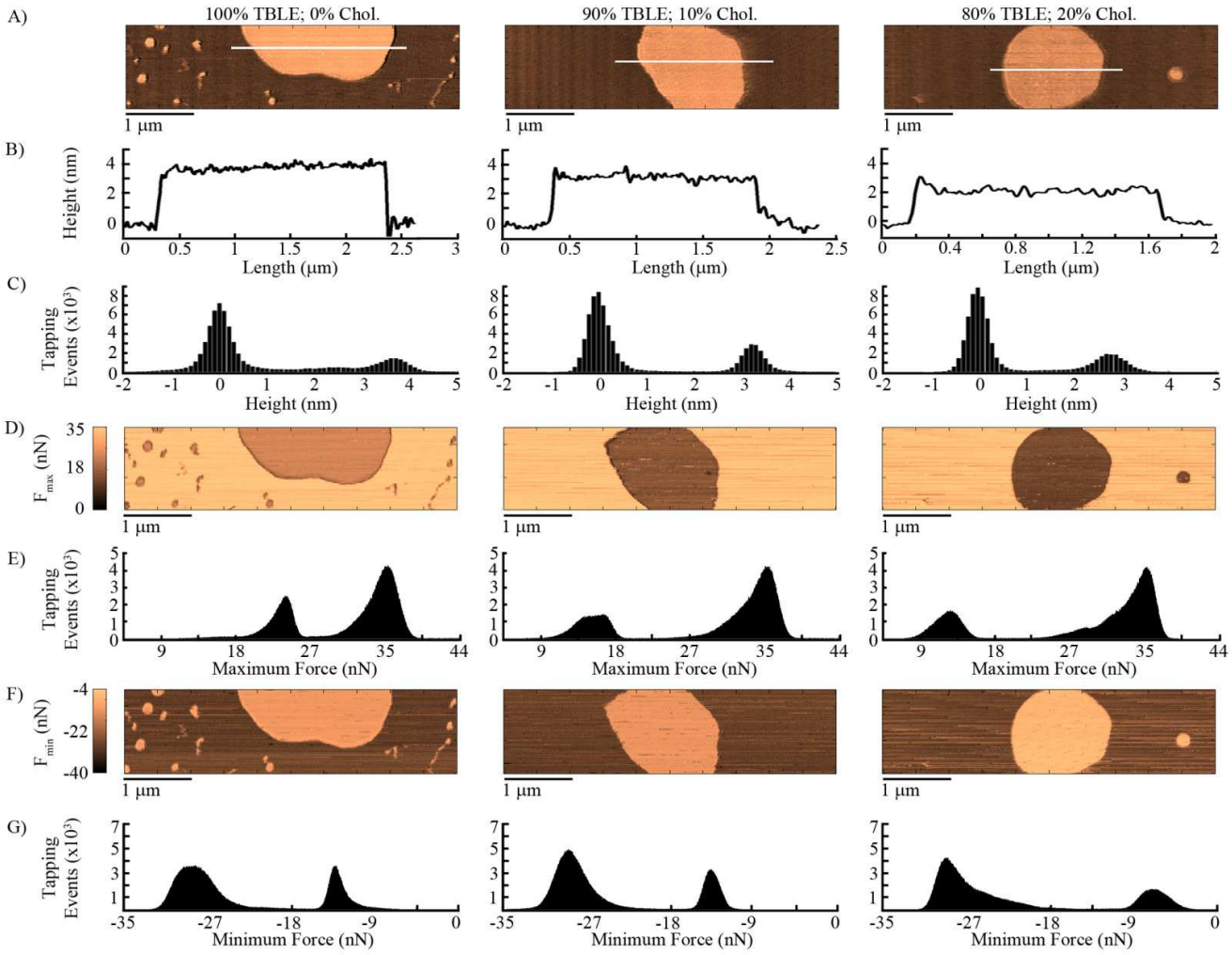

Figure 5. AFM and SPAM analysis of supported TBLE lipid bilayers with varying amounts of cholesterol (0%, 10%, and 20% by mass). (A) Topography images of lipid patches. The line in the image corresponds to the (B) height profile directly below each image. (C) Histograms of all of the height values of the pixels contained in the topography image. (D) Reconstructed F_{max} images associated with 100% TBLE and 0% cholesterol, 90% TBLE and 10% cholesterol, 80% TBLE and 20% cholesterol. (E) Histograms of the maximum tapping force associated with each F_{max} image. The peaks at 35 nN represent the force associated with the mica and the peaks to the left are associated with the bilayer. (F) Reconstructed F_{min} images associated with 100% TBLE and 0% cholesterol, 90% TBLE and 10% cholesterol, 80% TBLE and 20% cholesterol. (G) Histograms of the minimum tapping force associated with each F_{min} image. The peaks at -29 nN represent the force associated with the mica and the peaks to the right are associated with the bilayer.

this decrease in height could be due to either an increase in the Hamaker constant between the tip and bilayer or by a decrease in the Young's modulus. To determine the dominant contributor to the observed decreased height as a function of cholesterol content, the F_{max} and F_{min} for every tapping event was mapped to correspond directly to morphological features and analyzed (Figure 5 D-G and Figure 6). As the cholesterol content increases, the relative, average value of F_{max} associated with regions of lipid bilayer decreases with respect to the forces on mica. However, the relative, average value of F_{min} with respect to the forces measured on mica does not change when 10% exogenous cholesterol is added compared to pure TBLE. This suggests that the increased compression of the lipid bilayer (as measured by changes in height) was predominately due to changes in the Young's modulus induced by the addition of cholesterol. While the relative value of F_{min} for bilayer compared to mica increased in magnitude when 20% exogenous cholesterol is added, it was not enough of a change to account completely for the associated relative change in F_{max}. The forces are presented relative to the average tapping forces associated with imaging the exposed mica substrate. The average F_{max} and F_{min} for the mica surface were 35 and -29 nN, respectively.

4. CONCLUSIONS

A major thrust in the field of scanning probe techniques is to develop methods to simultaneously capture mechanical information about surfaces during standard imaging experiments. In TMAFM, this goal is becoming realizable due to the development of techniques with the ability to reconstruct the time-resolved force interaction between the tip and surface. Presented results and simulations demonstrate that the maximum and minimum observed tapping force for TMAFM operation in fluids is directly related to material properties such as Young's modulus and surface free energy between the tip and surface. As a result, these features of the time resolved tip/sample force interactions can be used to map relative changes in surfaces properties with nanoscale spatial resolution. Based on this principle, we have demonstrated the applicability of the SPAM technique, which enables the reconstruction of tapping forces from the deflection signal of a TMAFM experiment, to study the mechanical changes induced in supported lipid bilayer patches by the addition of exogenous cholesterol. However, to facilitate comparison, the imaging parameters (set point ratio, free amplitude, drive amplitude) should be maintained across experiments. The dynamics of lipid systems during cholesterol modulation are complex and it is well known that cholesterol depletion or enrichment has a global effect on cells [18-20]. Consequently, future cholesterol studies using SPAM will be performed with cells to determine the effects on not only the membrane, but the underlying cytoskeleton as well.

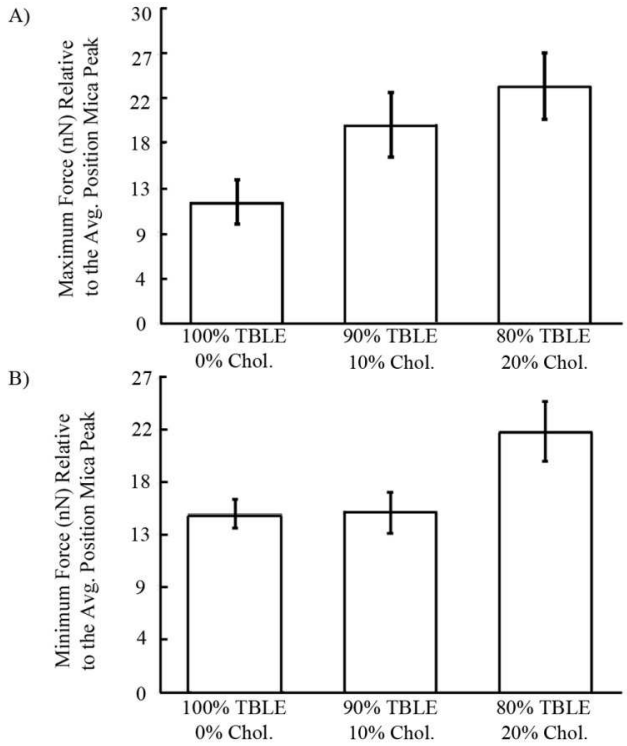

Figure 6. The average (A) F_{max} and (B) F_{min} associated with lipid bilayer patches with varying amounts of cholesterol.

5. ACKNOWLEDGMENTS

This work was funded by the Brodie Discovery and Innovation fund as well as the National Science Foundation (NSF#1054211). NSK was supported by a fellowship from the WVNano Initiative, which acknowledges support from the National Science Foundation (Cooperative Agreement 1003907). KMW was supported by the WVNano Initiative Research Experience for Undergraduates Program.

6. REFERENCES

[1] Kumar, B., Pifer, P. M., Giovengo, A. and Legleiter, J., 2010, "The effect of set point ratio and surface Young's modulus on maximum tapping forces in fluid tapping mode atomic force microscopy," J. Appl. Phys., 107, 044508.
[2] Legleiter, J., Park, M., Cusick, B. and Kowalewski, T., 2006, "Scanning probe acceleration microscopy (SPAM) in fluids: Mapping mechanical properties of surfaces at the nanoscale," Proc. Nat. Acad. Sci. (USA), 103, 4813-4818.
[3] Sahin O., Magonov S., Su C., Quate C.F. and O, S., 2007, "An atomic force microscope tip designed to measure time varying nanomechanical forces," Nat. Nanotechnol., 2, 507.
[4] Xu, X., Melcher, J., Basak, S., Reifenberger, R. and Raman, A., 2009, "Compositional Contrast of Biological Materials in Liquids Using the Momentary Excitation of Higher Eigenmodes in Dynamic Atomic Force Microscopy," Phys. Rev. Lett., 102, 060801.
[5] Xu, X., Melcher, J. and Raman, A., 2010, "Accurate force spectroscopy in tapping mode atomic force microscopy in liquids," Phys. Rev. B, 81, 035407.
[6] Solares, S.D., Chang, J., Seog, J. and Kareem, A.U., 2011, "Utilization of simple scaling laws for modulating tip-sample peak forces in atomic force microscopy characterization in liquid environments," J. Appl. Phys., 110,
[7] Kuhle A., Sorensen A. H., and Bohr, J., 1997, "Role of attractive forces in tapping tip force microscopy," J. Appl. Phys., 81, 6562.
[8] Salapaka, M. V., Chen, D. J. and Cleveland, J. P., 2000, "Linearity of amplitude and phase in tapping-mode atomic force microscopy," Phys. Rev. B: Condens. Matter Mater. Phys., 61, 1106-1115.
[9] Israelachvili, J. and Wennerstrom, H., 1996, "Role of hydration and water structure in biological and colloidal interactions," Nature (London), 379, 219-25.
[10] Derjaguin B. V., Muller, V. M., Toporov, Y.P., 1975, "Effect of contact deformations on the adhesion of particles," J. Colloid Interface Sci., 53, 314.
[11] Basak, S. and Raman, A., 2007, "Dynamics of tapping mode atomic force microscopy in liquids: Theory and experiments," Appl. Phys. Lett, 91, 064107.
[12] Xu, X., Carrasco, C., Jose, d. P. P., Gomez-Herrero, J. and Raman, A., 2008, "Unmasking imaging forces on soft biological samples in liquids when using dynamic atomic force

microscopy: a case study on viral capsids," Biophys. J., 95, 2520-2528.
[13] Legleiter, J. and Kowalewski, T., 2005, "Insights into fluid tapping-mode atomic force microscopy provided by numerical simulations," Appl. Phys. Lett., 87, 163120.
[14] Putman,C. A. J., Van der Werf, K. O., De Grooth, B.G., Van Hulst,N.F., and Greve,J., 1994, "Tapping mode atomic force microscopy in liquid," Appl. Phys. Lett., 64, 2454-6. Israelachvili, J., 1992, "Intermolecular & Surface Forces,"
[16] Hutter, J. L. and Bechhoefer, J., 1993, "CALIBRATION OF ATOMIC-FORCE MICROSCOPE TIPS," Rev. Sci. Instr., 64, 1868-1873.
[17] Kowalewski, T. and Legleiter, J., 2006, "Imaging stability and average tip-sample force in tapping mode atomic force microscopy," J. Appl. Phys., 99, 064903.
[18] Kwik, J., Boyle, S., Fooksman, D., Margolis, L., Sheetz, M. P. and Edidin, M., 2003, "Membrane Cholesterol, Lateral Mobility, and the Phosphatidylinositol 4,5-Biphosphate-Dependent Organization of Cell Actin," Proc. Nat. Acad. Sci. (USA), 100, 13964-13969.
[19] Mingzhai, S., Northup, N., Marga, F., Huber, T., Byfield, F. J., Levitan, I. and Forgacs, G., 2007, "The effect of cellular cholesterol on membrane-cytoskeleton adhesion," J. Cell Sci., 120, 9-9.
[20] Norman, L. L., Oetama, R. J., Dembo, M., Byfield, F., Hammer, D. A., Levitan, I. and Aranda-Espinoza, H., 2010, "Modification of Cellular Cholesterol Content Affects Traction Force, Adhesion and Cell Spreading," Cell. Mol. Bioeng., 3, 151-162.